Astron. Astrophys. 354, 497–503 (2000)

ASTRONOMY AND ASTROPHYSICS

VLBI observations of 3C 273 at 22 GHz and 43 GHz

II. Test of synchrotron self-Compton process

F. Mantovani[1], **W. Junor**[2], **I.M. M^{c}Hardy**[3], **and C. Valerio**[1]

[1] Istituto di Radioastronomia del CNR, via Gobetti 101, 40129 Bologna, Italy
[2] Institute for Astrophysics, University of New Mexico, Albuquerque, NM, USA
[3] Department of Physics and Astronomy, University of Southampton, UK

Received 25 June 1999 / Accepted 23 November 1999

Abstract. The VLBI observations at 22 GHz and 43 GHz of the quasar 3C 273 obtained during a multi-frequency campaign in late 1992 in the radio, millimetre and X-ray bands allow us to derive the components' angular sizes, their peak fluxes and turnover frequencies. Lower limits to the Doppler factors have been derived by comparing the observed X-ray fluxes with those predicted by the Synchrotron Self-Compton model. Independent estimates of the Doppler factors were obtained through the assumption of the energy equipartition between the particles and the magnetic field. Of the five components used to model the first two milli-arcseconds of the jet, apart from the core, two components are in equipartition and the remaining two, at larger distances from the core, have large Doppler factors and are mainly responsible for the X-ray emission due to the Synchrotron Self-Compton process.

Key words: radiation mechanisms: non-thermal – techniques: interferometric – galaxies: jets – galaxies: quasars: general – galaxies: quasars: individual: 3C 273 – radio continuum: galaxies

1. Introduction

There is a general agreement that most of the emission from blazars comes from a relativistic jet oriented close to the observer's line-of-sight. In this model, the emission from the radio through to the UV is synchrotron radiation and it is believed that the X and γ-ray emission is due to Compton up-scattering of low energy seed photons. The seed photons could arise externally to the jet, as in the External Compton Scattering or ECS model, where the photons arise from the accretion disc or broad line clouds (e.g. Melia & Königl 1989). However the most popular model is the Synchrotron Self-Compton (SSC) model where the seed photons are the synchrotron photons generated internally in the jet, which are then scattered to high energies by their parent electrons. This model is popular since, at some level, SSC scattering must occur.

Send offprint requests to: fmantovani@ira.bo.cnr.it

The SSC and ECS models, and variants thereof, such as the Mirror Compton Model (e.g. Ulrich et al. 1997), can, in principle, be distinguished by careful measurement of the lags, during outbursts, between various wavebands, principally the high and low energy bands, and by measurement of the relative amplitude of variability in the high and low energy bands (e.g. Marscher & Travis 1996; Ghisellini & Maraschi 1996). However arranging monitoring in a number of different wavebands is not trivial and has rarely been achieved (e.g. M^{c}Hardy et al. 1999).

An alternative method of testing the SSC model is by measurement of the physical parameters of the possible sites of synchrotron emission by VLBI multi-frequency radio observations of the cores of compact superluminal radio sources. From such observations we can measure the angular size, radio spectrum and self-absorption frequency of the various radio components. If, in addition, the relativistic Doppler factor has been estimated from the motion of radio components, then the SSC X-ray flux can be accurately predicted (e.g. Marscher 1983). Thus a combination of VLBI and X-ray observations can provide an excellent test of the SSC model. Of course, in most situations some important parameter, usually the Doppler factor, is not well determined. In that case the Doppler factor can be very well constrained from the combination of VLBI and X-ray observations. A consistency check can be achieved by comparing the derived Doppler factor with its estimate derived by equipartition arguments (Readhead 1994). The comparison can enable us to distinguish which, if any, of the radio components is most likely to be the major source of X-ray emission.

In this paper, we compare the X-ray and VLBI observations of 3C 273, one of the brightest and best-studied of the superluminal radio sources, in order to test the SSC model and to determine the origin of the X-ray emission in 3C 273.

The VLBI observations of 3C 273 at 22 GHz and 43 GHz presented in Mantovani et al. (1999; hereafter Paper I), were performed as part of a multi-frequency campaign carried out from December 12, 1992 to January 24, 1993. Over this period 3C 273 was monitored every 2 days with the PSPC of ROSAT in the $0.1 - 2.4\,keV$ band (Leach et al. 1995), at nearly 1 day intervals at 2, 1.1, 0.8, 0.45 mm with the JCMT (Mauna Kea), IRAM and the Kitt Peak telescope (M^{c}Hardy et al. 1994).

Table 1. Component parameters

comp	$\langle\theta_1\rangle$ (mas)	$\langle\theta_2\rangle$ (mas)	$\langle 1.8\sqrt{\theta_1\theta_2}\rangle$ 22 GHz (mas)	$\langle\theta_1\rangle$ (mas)	$\langle\theta_2\rangle$ (mas)	$\langle 1.8\sqrt{\theta_1\theta_2}\rangle$ 43 GHz (mas)	$\langle r\rangle$ (mas)	$\langle PA\rangle$ (deg)	S_{22} (Jy)	S_{43} (Jy)	α
1	0.15	0.30	0.38	0.16	0.34	0.42			1.82	2.57	–0.52
2	0.19	0.41	0.50	0.15	0.33	0.40	0.34	–100	4.50	2.02	1.20
3	0.23	0.45	0.58	0.29	0.48	0.67	0.70	–115	8.46	4.45	0.97
4	0.28	0.44	0.63	0.25	0.49	0.63	1.29	–121	2.76	0.83	1.81
5	0.27	0.47	0.64	0.25	0.41	0.57	1.75	–108	3.05	1.06	1.60

No large flares were seen in that period but variations in both wavebands of ∼30% on few day timescales are apparent. The X-ray spectrum consists of 2 power-law components with the harder component dominating above 0.5 keV. There is a very little correlation between the variability of the soft and hard components. The soft component does not correlate with the millimeter variations. The hard component may correlate reasonably with the millimetre variations, leading the millimetre by about 10 days but the correlation is weak and may be the result of chance statistical fluctuation. However, M^{c}Hardy et al. (1999) have demonstrated that a strong relationship does exist between the X-ray emission and the infrared band in 3C 273, and the infrared is almost certainly just a tracer for the whole infrared to millimetre synchrotron spectral component.

The jet structure of 3C 273 obtained by the VLBI observations, discussed in Paper I, does not dramatically change in the observing window of 43 days. Good evidence was found for a bending of the jet, beginning inside the first parsec from the core; this behaviour strongly suggests a precessing jet. The possibility that the morphology in 3C 273 can also be modelled with Kelvin-Helmholtz instabilities cannot be excluded, however.

The model-fitting of the jet structure makes it possible to follow the changes in separation of the components with respect to the core. Moreover, we can derive the components' angular sizes (Sect. 2.1) and their peak flux densities and turnover frequencies (Sect. 2.2). These parameters are fundamental to the analysis in terms of the SSC process (Sect. 2.3). In Sect. 3 the results will be discussed.

2. Parameters derived from the observations

2.1. Angular sizes

The source 3C 273 was observed with an array consisting of the VLBA plus Effelsberg, Medicina and Noto at 22 GHz, while the stand-alone VLBA was used at 43 GHz. The structure of the jet of 3C 273 has been modelled with Gaussian components. The model-fitting was performed on the final self-calibrated visibilities of each data set (see Paper I). The inner two milliarcseconds (mas), have been modelled with five components at both 43 GHz and 22 GHz with a good formal agreement, χ^2_ν, between data and model. The ratio between the total flux density from the hybrid images and the flux density obtained adding up the flux density of each individual components in the related model was always close to 1. The models obtained from the 22 GHz data sets, using the visibilities in the baseline range $\leq$450 Mλ to match the resolution to that of the 43 GHz observations, will also be used in the following analysis.

The Gaussian components found in the models are compact compared to the synthesized beam and their angular sizes do not change noticeably between epochs. Consequently, the mean value of the angular sizes found for each component will be adopted. The major axis and the minor axis FWHMs, θ_1 and θ_2 respectively, were then averaged geometrically. To be conservative in the calculation of the X-ray emission by the SSC process, the mean angular sizes of the components are obtained with the relation $\theta = 1.8\sqrt{\theta_1\theta_2}$, to convert the deconvolved Gaussian diameters to the optically thin sphere diameter. The angular sizes in Table 1 computed for each component of the 22 GHz and the 43 GHz models respectively, are similar. In order to compute the X-ray emission by SSC process, in the following we will adopt the angular sizes obtained by modelfitting the 43 GHz data. The observations at that frequency had a better *uv* coverage and comparable resolution in the North-South and East-West directions; this allows us to derive more reliable parameters. The mean flux densities values for each of the components is also reported in Table 1.

The Table 1 is organized as follows: Column 1, component's label; Columns 2 and 3, minor and major axis FWHMs at 22 GHz respectively; Column 4, angular sizes at 22 GHz; Columns 5 and 6, minor and major axis FWHMs at 43 GHz respectively; Column 7, angular sizes at 43 GHz; Columns 8 and 9 mean separation and Position Angle of each component from component 1 taken as the reference point; Columns 10 and 11, mean flux density of the components at 22 GHz and 43 GHz respectively (see below); Column 12, spectral index α ($S \propto \nu^{-\alpha}$) between the two frequencies.

2.2. Radio spectrum

The X-ray emission due to SSC is strongly dependent on the self-absorption turnover frequency ν_m and on the flux density S_m at ν_m. The present VLBI observations at 22 GHz and 43 GHz provide simultaneous flux densities measurements with similar resolving power. Simultaneous observations with similar resolution at lower frequency (i.e. VSOP observations at 5 GHz), as are possible now, would have been ideal for a proper estimate of both ν_m and S_m. These parameters will be derived here with the following approach.

The total power flux densities measurements of 3C 273 at various frequencies made in the period of our observations were

Table 2. Parameters and derived physical quantities for each of the components

comp	ν_m GHz	S_m Jy	S_X(1keV) μJy	S_X(0.1-2.4keV) erg/(sec cm^2)	δ_X	δ_{eq}	T_b °K	$(T_b)_{eq}$ °K
1	90	3.5	4.5×10^{-7}	3.3×10^{-18}	> 0.01	0.01	3.0×10^{9}	4.3×10^{10}
2	15	5	16	1.2×10^{-10}	> 1.1	2.2	1.8×10^{11}	4.1×10^{10}
3	14	12	35	2.7×10^{-10}	> 1.2	2.5	1.7×10^{11}	5.2×10^{10}
4	6	15	2.5×10^{5}	1.9×10^{-6}	> 3.8	29.5	1.3×10^{12}	5.5×10^{10}
5	6	15	2.2×10^{5}	1.6×10^{-6}	> 4.0	37.4	1.6×10^{12}	5.5×10^{10}

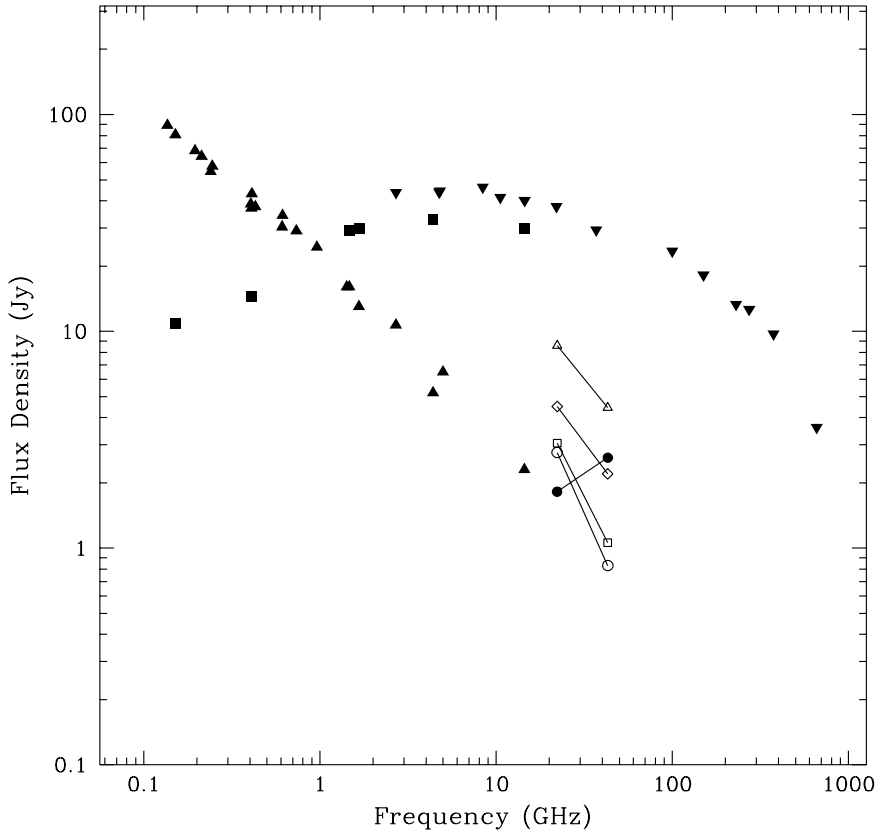

Fig. 1. Radio spectrum of 3C 273. Symbols: ▲ flux density from the arcsecond scale jet as in Conway et al. (1993), ▼ total flux density as from von Montigny et al. (1997), ■ flux density from the arcsec core. The flux densities from the various components are • comp. 1, ◇ comp. 2, △ comp. 3, ○ comp. 4, □ comp. 5 respectively.

taken from the compilation by von Montigny et al. (1997). The appropriate flux density measurements for the arcsecond scale jet, as given by Conway et al. (1993), have been subtracted from the total flux measurements since the arcsecond jet has an optically-thin spectrum and its flux density should be fairly constant in time. What remains is the emission from the core and milliarcsecond jet at the time of our observations. The spectra are plotted in Figs. 1 and 2. The integrated spectrum of the core and milliarcsecond jet has been reconstructed, by adding up the spectra which the five components should have, given the VLBI flux density measurements which we obtained at the two frequencies. The self-absorption turnover frequency ν_m and flux density S_m from the spectral decomposition are reported in Table 2.

Component 1 is the only one which shows an inverted spectra and should be the core. Its turnover frequency of ∼90 GHz is confirmed by quasi-contemporary VLBI observations at 86 GHz made on January 1993 (T. Krichbaum, private communication) in which the unresolved core component has a flux density of 3.6 Jy. The 86 GHz model shows two more components at a separation of 0.39 mas and 1.4 mas from the core respectively. Their positions correspond to the positions of components 3 and 4 in our model(s) and they have flux densities of 2.8 Jy and 0.9 Jy respectively. These last values fit with the measured trend for the optically-thin part of the spectrum of those components. Component 2 is weaker than component 3 and the turnover frequencies of both components are at ∼15 GHz. Components 4 and 5 have spectra with turnovers at much lower frequencies than components 2 and 3 and the optically-thin spectra have steep gradients. The total correlated flux density at both 22 GHz and 43 GHz does not account for the expected emission at arcsecond scale resolution from the core at those frequencies. The missing flux density must come from the region of the jet intermediate between the mas and the arcsecond scales; this part cannot be properly imaged by the available interferometers. A

full discussion of the amplitude calibration can be found in Paper I.

2.3. X-ray emission by synchrotron self-Compton process

Monitoring observations from radio through millimeter wavelengths have shown many blazars have a characteristic behaviour – flares with a delayed broader peak relative to the higher frequencies, with a slow decline thereafter. From X-ray monitoring observations on 3C345, Unwin et al. (1997) found that the decline in X-ray flux is correlated with the radio flux at frequencies above 37 GHz. This correlation is strong evidence that X-ray emission originates in the parsec scale jet. In Paper I, we showed that the parsec-long radio jet in 3C 273 could be modelled with five well-separated components. Let us assume that these components are homogeneous and spherical, with tangled magnetic fields and high-energy electrons which follow an isotropic energy distribution ($N(E) = N_0 E^{-(2\alpha+1)}$). The electrons produce radio emission by synchrotron radiation and produce at least part of the X-ray flux by inverse Compton scattering of their own synchrotron photons. The electron in the jet may also produce X-rays by inverse Compton scattering of other low energy seed photons, eg from nuclear accretion disc, or by scattering synchrotron jet photons which have been reflected back to the jet from nearby gas clouds (Ulrich et al. 1997).

The monochromatic SSC X-ray flux at a frequency ν_X (keV) produced by such a synchrotron source with angular diameter θ (mas), redshift z, spectral index α, break frequency ν_2 (GHz), self-absorption turnover frequency ν_m (GHz) and flux density S_m (Jy) is (see Marscher 1983):

$$S_X = h(\alpha) ln(\frac{\nu_2}{\nu_m}) \theta^{-2(2\alpha+3)} \nu_m^{-(3\alpha+5)} S_m^{2(\alpha+2)} \nu_X^{-\alpha} [\frac{1+z}{\delta}]^{2(\alpha+2)} \mu Jy \quad (1)$$

where $h(\alpha)$ is a dimensionless parameter depending on the spectral index ($\log h(\alpha) \approx -0.62\alpha + 2.24$, with $0.4 \leq \alpha \leq 1.0$) and δ is the Doppler factor. A value of 1000 GHz was adopted for ν_2 (see von Montigny et al 1997).

The resulting expected monochromatic X-ray fluxes (in μJy) from each component are given in Table 2, and have been computed assuming component spectral indices equal to 1 and Doppler factors equal to 1. In Table 2 we also give the expected fluxes, in erg/(sec cm^2), integrated over the 0.1–2.4 keV ROSAT observing band, i.e.

$$S_X(0.1 - 2.4\ KeV) = f(\alpha) S_{1keV}(\mu Jy) \times 10^{-29} ergs/(cm^2 sec) \quad (2)$$

where f(α) is a function of the spectral index which becomes 7.6×10^{17} for $\alpha = 1$, with the assumption that $\langle\nu\rangle = 2.4\times10^{17}$ Hz, i.e. an energy of 1 keV.

2.4. Doppler factors from SSC

The predicted Inverse Compton X-radiation should not exceed the observed X-ray flux. Since we have simultaneous radio and X-ray measurements, lower limits to the Doppler factors for each of the five components in the parsec-scale jet can be derived. The self-Compton X-ray fluxes for components 1 to 5 have been calculated and have been compared to the X-ray flux detected by ROSAT. Leach et al. (1995) have noted a mean variability on the counts rate of $\sim$8% on short, two day time scales. Such a fluctuation is ignored in the following discussion. Those authors have also pointed out the lack of correlation between the variations of the X-ray emission in the 0.1–0.3 keV and 1.5–2.4 keV, which might indicate that two distinct mechanisms of emission exist. They suggest that the X-ray spectrum is formed by two components with different power law spectra with the same intensity at about 1 keV. The soft component is probably due to inverse Compton scattering of UV photons from the accretion disk, while the hard component with spectrum $\sim$0.5 is due to inverse Compton scattering of their own synchrotron radiation by the electrons in the relativistic jet. This hypothesis is supported by two facts: (1) the mm-band emission during the multi-band campaign (M^{c}Hardy et al. 1994) is possibly correlated to the light curve of the 'hard' component of the X-ray emission; this component is probably due to SSC and (2) correlated IR/X-ray variability in 3C 273 (M^{c}Hardy et al. 1999). Thus we consider only the hard component ($S_{Xhard} = 7.7 \times 10^{-11} erg/cm^2 s$) to be due to the SSC process in order to obtain lower limits to the Doppler factors listed in Table 2.

The ratio between the X-ray flux density expected from SSC ($S_X(0.1-2.4keV)$ and the X-ray emission detected by ROSAT, is proportional to $(\delta_X)^{2(\alpha+2)}$, where δ_X is the Doppler factor. The spectral index for each component is listed in Table 1; a spectral index $\alpha = 0$ was adopted for component 1 (the core). Furthermore, the calculated X-ray flux cannot be larger than the observed value, so equating the calculated and measured flux densities yields δ_{min}, a lower limit to δ. The limits obtained for δ_X are reported in Table 2.

2.5. Doppler factors from equipartition

An independent method of estimating the Doppler factor in powerful extragalactic radio sources is the use of the equipartition condition. Since we know the components' angular diameters, turnover frequencies and flux densities, it is possible to compute the energy density content in the relativistic electrons u_e and in the magnetic field u_m. If we assume that the source is in equipartition (i.e. Readhead 1994), the Doppler factors of the components can be derived from the relation:

$$E_{em} = \frac{u_e}{u_m} \simeq 3.0 \times 10^{10} (\frac{H_\circ}{100}) D^{-1} \nu_m^{-17.5+\alpha} (GHz) \theta^{-17} (mas) S_m^8 (Jy) \frac{(1+z)^9}{\delta^7} \quad (3)$$

where, of course, $E_{em} = 1$ and in which:

$$D = \frac{q_\circ z + (q_\circ - 1)(\sqrt{1+2q_\circ z} - 1)}{q_\circ^2} \quad (4)$$

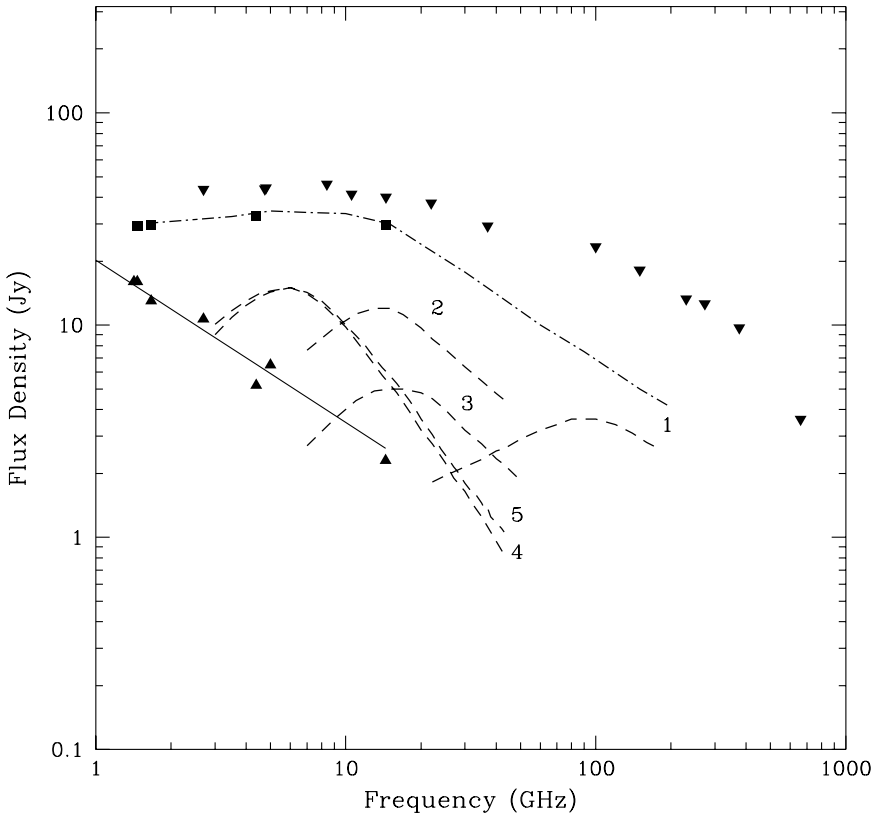

Fig. 2. Decomposition of the spectrum of 3C 273. Symbols: ▲ flux density from the arcsecond scale jet as in Conway et al. (1993), ▼ total flux density as from von Montigny et al. (1997), ■ flux density from the arcsec core. The spectra of the five components are plotted. The dotted line represents the spectra sum of the five components.

where ($H_0 = 100\,km\,s^{-1}\,Mpc^{-1}$, $q_0 = 0.5$). The Doppler factors from equipartition δ_{eq} are reported in Table 2.

2.6. Brightness temperatures of the components

The lower limits to the brightness temperature, T_b, for each of the components along the jet of 3C 273 can be computed with the expression:

$$T_b = 1.41 \times 10^9 (1+z)(\frac{S_m}{Jy})(\frac{\theta}{mas^2})^{-2}(\frac{\lambda_m}{cm})^2 \qquad (5)$$

where $\theta = 1.8\sqrt{\theta_1\theta_2}$ is the components' angular size and θ_1 and θ_2 are the mean minor and the mean major axis angular sizes of each component, S_m is the turnover flux density, λ_m the turnover wavelength and z is the redshift. The derived values are listed in Table 2, together with the brightness temperature from equipartition $(T_b)_{eq}$ obtained by the Eq. (4*b*) in Readhead (1994) when the Doppler factor of the emission region is taken to be equal to 1.

As expected, the equipartition requirements give a limit to the brightness temperature of $\simeq 10^{11}$ °K, while the values for the brightness temperature in the rest frame of the source T_b, given by Eq. (5), are in the range from $\sim 10^{10}$ °K for the core to values slightly exceeding the IC limits for the outer components 4 and 5.

Table 3. Derived quantities

comp	$\|r\|$ mas/yr	β_{app} mas/yr	β_{min}	γ_{min}
2	0.82	5.5	0.984	5.6
3	0.44	3.0	0.949	3.2
4	1.57	10.6	0.996	10.6
5	1.51	10.2	0.995	10.2

2.7. Apparent speed, γ factor and the angle to the line of sight

From the observations presented in Paper I, we were able to measure the apparent speeds of the inner jet components in orthogonal directions. The values obtained, reported in Table 3, are generally consistent with those available in literature (i.e. Zensus et al. 1990). The apparent speed $\beta_{app} = v_{app}/c$ and the apparent γ factor can be calculated. They are listed in Table 3. That calculation is, of course, valid only if the apparent component velocities are due to bulk motion of the components and not if the motions represent enhanced emission regions caused by the movement of Kelvin-Helmholtz instabilities along the jet. Using the lower values for β_{app} and γ_{min} gives the angle of the jet respect to the line of sight θ_{obs} in the range $15° \leq \theta_{obs} < 25°$. Using the higher values we obtain $2° \leq \theta_{obs} < 10°$.

From these values it is possible to estimate the Doppler factor range with the expression

$$\delta = [\gamma_{min}(1 - \beta_{min} cos\theta)]^{-1} \qquad (6)$$

With $\beta_{min} = 0.949$ and $\theta_{obs} = 25^\circ$ we obtain $\delta = 2.2$ and with $\beta_{min} = 0.996$ and $\theta_{obs} = 2^\circ$ we obtain $\delta = 20.5$.

3. Discussion

M^{c}Hardy et al. (1999) have recently shown that the medium energy X-ray (3–20 keV) from the NASA Rossi X-ray Timing Explorer observations and the near infrared fluxes from the UK Infrared Telescope (UKIRT) in the quasar 3C 273 are higly correlated. The lag between the IR and the X-ray bands is very small but, in at least the first flare observed by M^{c}Hardy et al., the IR leads the X-ray emission by $\sim 0.75 \pm 0.25$ days. This lag rules out the External Compton process but is consistent with the SSC model or, possibly, the Mirror Compton model.

On the assumption that the X-ray emission is produced by the SSC mechanism we have combined the radio observations with the contemporary X-ray observations to derive physical parameters of the milliarcsecond scale jet in 3C 273, particularly the Doppler factors of the radio components.

There is other evidence that the X-ray emission in blazars originates in a parsec scale jet. For example, in the case of 3C345, Unwin et al. (1997) show that the X-ray flux density measurements are directly correlated with the total flux density at frequencies above 37 GHz, both in amplitude range and variability. The predicted X-ray emission strongly depends on the angular size, turnover frequency and flux density of the radio components. Of those parameters, the angular size is the only one which comes directly from the present observations. It is worth noting that the usefulness of those measurements are affected by practical limitations. The maximum available baseline length, for example, limits the achievable resolution of the interferometer, so that the given angular sizes can be considered as upper limits only.

The turnover frequency and flux density for each of the components are more difficult to determine. The procedure followed in Sect. 2.2 allows us to estimate the arcsecond core spectrum of 3C 273 at the time of these VLBI observations using the mas components along the jet. The amplitude calibration of these observations has been discussed in Paper I. The missing flux at high frequencies should come from the extended structure of the jet, resolved out by these VLBI observations. The emission from the five components conspires in such a way that the almost flat spectrum of the core is reproduced.

The most relevant results from the SSC model and equipartition arguments, which are listed in Table 2, allow us to say that:

(a) component 1 (the core) is probably inhomogenous and there are no indications of relativistic effects. The X-ray emission from the core is rather weak but the computation has been done considering the core as an homogeneous expanding sphere. However, Unwin et al. (1985, 1997) have shown that the cores in 3C 273 and in 3C345 cannot be the origin of their X-ray emissions, even applying the probably more relevant inhomegeneous-jet model of Königl (1981). The model under-estimates the X-ray flux from the core for any possible combination of parameters derived from the observations.

(b) components 2 and 3 show Doppler factors from SSC and equipartition that are similar and close to 1. This could mean that components 2 and 3 are stationary, are the origin of the observed X-ray emission, and are close to equipartition. Alternatively if the Doppler factor for these components is > 1, as seems reasonable given that the derived Doppler factors for all of the other components apart from the core are > 1, then these components cannot be important sources of X-ray emission.

(c) components 4 and 5 show very large valus of δ_X. It follows that relativistic effects must be present. Moreover, δ_X and δ_{eq} are rather different from each other, indicating that the components might not be in equipartition.

(d) the brightness temperatures for components 4 and 5 slightly exceed the Compton limits. These results and those in (c) are mainly due to the low values for ν_m that result from the decomposition of the spectrum. It might be noted that these two components do have rather steep optically-thin spectral indices. As mentioned in chapter 2.2, the steepening of the spectrum of component 4 is supported by observations at 86 GHz. Moreover, a less steep spectrum implies a shift of the turnover frequency to even lower frequencies, to account for the arcsecond flux density.

The X-ray emission probably comes mainly from components 4 and 5. Those two components are at the largest separation from the core. Similar results are found by Unwin (1997) for 3C345, in which component C7, and not the unresolved core region, is the dominant source of X-ray emission in the period of their observations.

The present results are in a similar vein. The X-ray emission increases with the separation of the components from the inhomogeneous core. With increasing separation from the core region, the components show a decreasing value for the turnover frequency and an increase in the turnover flux density. The more distant components have much higher values for the Doppler factor derived from equipartition arguments than derived from SSC modelling and so are very likely not in equipartition. The increase in values of both SSC and equipartition Doppler factors might simply mean that the jet axis bends closer towards the observers line of sight at larger distances from the core.

Acknowledgements. The authors would like to thank Roberto Fanti for many useful discussions and Thomas Krichbaum for the 86 GHz VLBI model for 3C 273 kindly provided prior to publication.

References

Conway R.G., Garrington S.T., Perley R.A., Biretta J.A., 1993, A&A 267, 347
Ghisellini G., Maraschi L., 1996, ASP Conf. Ser. 110, 436
Königl A., 1981, ApJ 243, 700
Leach C.M., M^{c}Hardy I.M., Papadakis I.E., 1995, MN 272, 221
Mantovani F., Junor W., Valerio C., M^{c}Hardy I., 1999, A&A 346, 397
Marscher A.P., 1983, ApJ 264, 296
Marscher A.P., Travis J.P., 1996, A&AS 120, 537
M^{c}Hardy I.M., Papadakis I., Leach C.M., et al, 1994, In: Courvoisier T.J.-L., Blecha A. (eds.) IAU Symposium 159, p. 193
M^{c}Hardy I.M., Lawson A.J., Newsam, et al., 1999, MN, in press
Melia F., Königl A. 1989, ApJ 340 162

Readhead A.C.S., 1994, ApJ 426, 51
Ulrich M.H., Maraschi L., Urry C.M., 1997, ARA&A 35, 445
Unwin S.C., Cohen M.H., Biretta J.A., et al., 1985, ApJ 289 109.
Unwin S.C., Wehrle A.E., Lobanov A.P., et al., 1997, ApJ 480, 596
von Montigny C., Aller H., Aller M., et al., 1997, ApJ 483, 161
Zensus J.A., Unwin S.C., Cohen M.H., Biretta J.A., 1990, AJ 100, 1777